Fermi surface reconstruction in hole-doped t-J models without long-range antiferromagnetic order

Matthias Punk and Subir Sachdev
Department of Physics, Harvard University, Cambridge, Massachusetts 02138, USA
(Received 12 March 2012; published 11 May 2012)

We calculate the Fermi surface of electrons in hole-doped, extended t-J models on a square lattice in a regime where no long-range antiferromagnetic order is present, and no symmetries are broken. Using the "spinon-dopon" formalism of Ribeiro and Wen, we show that short-range antiferromagnetic correlations lead to a reconstruction of the Fermi surface into hole pockets which are not necessarily centered at the antiferromagnetic Brillouin zone boundary. The Brillouin zone area enclosed by the Fermi surface is proportional to the density of dopants away from half-filling, in contrast to the conventional Luttinger theorem, which counts the total electron density. This state realizes a "fractionalized Fermi liquid" (FL*), which has been proposed as a possible ground state of the underdoped cuprates; we note connections to recent experiments. We also discuss the quantum phase transition from the FL* state to the Fermi liquid state with long-range antiferromagnetic order.

DOI: 10.1103/PhysRevB.85.195123 PACS number(s): 71.10.Hf, 71.18.+y, 74.72.Kf, 75.10.Kt

I. INTRODUCTION

The nature of electronic Fermi surfaces in strongly correlated metals, in particular underdoped cuprates, has been the subject of intensive debate for many years. Recent observations of pocketlike Fermi surfaces in quantum oscillation experiments[1–5] as well as new angle-resolved photoemission measurements[6] have triggered a renewed theoretical interest in this matter.[7–9]

One possible, well-known route to a Fermi surface reconstruction is the onset of spin-density wave (SDW) order, which breaks a large Fermi surface into small electron and hole pockets centered at the magnetic Brillouin zone boundary.[10,11] In fact, many of the unresolved theoretical problems in strongly correlated electron materials, from heavy-fermion compounds to high-T_c cuprates, are related to the fate of electronic excitations close to antiferromagnetic quantum-critical points.[12] It has been been argued, however, that the critical point between a metal with a large Fermi surface and an antiferromagnetic metal with small Fermi pockets may be replaced by a new intermediate phase, the so-called fractionalized Fermi liquid (FL*),[13,14] which exhibits small pockets similar to the antiferromagnetic metal, but breaks no symmetries: summaries of these arguments, and of previous theoretical work, can be found in two recent reviews.[15,16]

The simplest picture of the FL* phase appears in the context of Kondo lattice models coupling a lattice of localized f moments and a conduction band of itinerant c electrons. There are two important energy scales to consider: the Kondo exchange J_K between the f moments and the c electrons, and Heisenberg exchange J_H between the f moments. If $J_K \gg J_H$, then f moments are "Kondo screened" by the conduction electrons, leading to a Fermi liquid ground state with Fermi surfaces enclosing the traditional Luttinger volume, which counts the density of *both* the f and c electrons; the only memory of the localized nature of the underlying f electrons is that electronic quasiparticles near the Fermi surface have an effective mass which is much larger than the bare electron mass, and so this phase is often referred to as a "heavy" Fermi liquid. However, in the opposite parameter regime $J_H \gg J_K$, other phases can appear. The most natural possibility is the appearance of magnetic order of the f moments, but let us assume the f-f couplings are sufficiently frustrated so that this does not happen. Then, the f moments may form a spin liquid, which does not break any symmetries of the lattice Hamiltonian. The formation of the spin liquid also quenches the Kondo effect, and so the effective value of J_K does *not* renormalize to infinity as it does in the single impurity Kondo model.[13,14,17] The c electrons are now only weakly coupled to the f spin liquid, and so the c electrons form a "small" Fermi surface that encloses a volume controlled only by the density of c electrons, which violates the traditional Luttinger count. This is the FL* metal.

This paper describes a FL* state in a *single*-band model appropriate for the cuprate superconductors. Previous studies[18,19] realized such a state by initially fractionalizing the electron into a neutral $S = 1/2$ spinon and a spinless "holon" carrying electromagnetic charge. The spinons eventually became the excitations of a "background" spin liquid, analogous to the spin liquid of the f electrons above, and the holons eventually captured a spinon to reconstitute as electronlike particles, which occupied the states inside a small Fermi surface. Because of this somewhat intricate sequence of transformations, the description of the FL* state was only achieved in a semiphenomenological manner.

Here, we will provide a more direct and quantitative description of the FL* state in a single-band model. The key step will be a rewriting of the single-band degrees of freedom in a manner which mimics those of the Kondo lattice. Such a formulation is provided by the representation of Ribeiro and Wen[20] in which the electron fractionalizes into a neutral spinon and a "dopon," which has the same quantum numbers as the electron.

The rest of the paper is organized as follows. In Sec. II, we introduce the extended t-J model in the representation of Ribeiro and Wen,[20] which is ideally suited for our purposes. Section III deals with our approach to construct FL* ground states and presents results for the shape and position of the electronic Fermi surface. Section IV describes the Fermi surface evolution from the FL* state to the Fermi liquid state with long-range antiferromagnetic order, along with a discussion of the quantum-critical properties. We summarize our results, and note connections to recent experiments in Sec. V.

II. MODEL

In the following, we study ground states of extended t-J Hamiltonians on the square lattice

$$H = -\frac{1}{2}\sum_{ij} t_{ij}(\tilde{c}^\dagger_{i\sigma}\tilde{c}_{j\sigma} + \text{H.c}) + \frac{1}{2}\sum_{ij} J_{ij}\left(\mathbf{s}_i\cdot\mathbf{s}_j - \frac{1}{4}n_i n_j\right), \tag{2.1}$$

where $\tilde{c}^\dagger_{i\sigma}$ ($\tilde{c}_{i\sigma}$) denotes the Gutzwiller projected creation (annihilation) operator of electrons with spin σ on lattice site i, $\mathbf{s}_i = \tilde{c}^\dagger_{i\alpha}\boldsymbol{\sigma}_{\alpha\beta}\tilde{c}_{i\beta}$ is the electron spin operator, and $n_i = \tilde{c}^\dagger_{i\sigma}\tilde{c}_{i\sigma}$ the electron number operator (here and in the following, we sum over repeated spin indices). We are interested in describing possible ground states slightly below half-filling $n = 1 - x$, where the density of doped holes is small $x \ll 1$, but large enough to destroy any long-range magnetic order. In addition, these ground states should not break any lattice symmetries. In particular, we want to show that strong short-range antiferromagnetic correlations already lead to a reconstructed Fermi surface consisting of small hole pockets, the area of which is proportional to the dopant density x, instead of $1 - x$ as for conventional Fermi liquids. Such ground states realize a fractionalized Fermi liquid.[13,14]

Our starting point is the spinon-dopon formulation of the t-J model developed by Ribeiro and Wen.[20] In this representation, the elementary excitations are spinons, which carry spin-1/2 but no charge, and dopons, which carry spin-1/2 and charge. Accordingly, Ribeiro and Wen introduce two degrees of freedom per lattice site, a "localized" spin-1/2 as well as a fermionic spin-1/2 degree of freedom (the dopon), representing a doped charge carrier. A physical hole corresponds to a singlet of a lattice spin and a dopon. The correspondence between single-site basis states is shown in Table I. Following this approach, the t-J Hamiltonian in Eq. (2.1) takes the form[20]

$$\begin{aligned} H = &\sum_{ij}\frac{J_{ij}}{2}\left(\mathbf{S}_i\cdot\mathbf{S}_j - \frac{1}{4}\right)\mathcal{P}(1 - d^\dagger_{i\alpha}d_{i\alpha})(1 - d^\dagger_{j\beta}d_{j\beta})\mathcal{P} \\ &+ \frac{1}{2}\sum_{ij}\frac{t_{ij}}{2}\mathcal{P}\Big[\frac{1}{4}d^\dagger_{i\alpha}d_{j\alpha} - \frac{1}{2}(d^\dagger_{i\alpha}\boldsymbol{\sigma}_{\alpha\beta}d_{j\beta})\cdot(\mathbf{S}_i + \mathbf{S}_j) \\ &+ d^\dagger_{i\alpha}d_{j\alpha}\mathbf{S}_i\cdot\mathbf{S}_j + i(d^\dagger_{i\alpha}\boldsymbol{\sigma}_{\alpha\beta}d_{j\beta})\cdot(\mathbf{S}_i\times\mathbf{S}_j) + \text{H.c.}\Big]\mathcal{P} \\ &- \mu\sum_i d^\dagger_{i\alpha}d_{i\alpha}\,. \end{aligned} \tag{2.2}$$

TABLE I. Single-site basis-state correspondence: t-J model versus spinon-dopon representation.

t-J	Spinon-dopon
$\lvert\uparrow\rangle_i$	$\lvert\uparrow 0\rangle_i$
$\lvert\downarrow\rangle_i$	$\lvert\downarrow 0\rangle_i$
$\lvert 0\rangle_i$	$(\lvert\uparrow\downarrow\rangle_i - \lvert\downarrow\uparrow\rangle_i)/\sqrt{2}$
Unphys.	Triplet states
Unphys.	Doubly occupied dopon

Here, $\mathcal{P} = \prod_j(1 - d^\dagger_{j\uparrow}d_{j\uparrow}d^\dagger_{j\downarrow}d_{j\downarrow})$ denotes the Gutzwiller projector for the fermionic spin-1/2 operators $d^\dagger_i$ and d_i that create or annihilate a dopon on lattice site i, and we added a chemical potential μ for the dopons. Note again that the spins $\mathbf{S}_j$ on each lattice site j are independent, localized spin-1/2 degrees of freedom and are not associated with the spin of the dopons. This representation of the t-J model is faithful in the sense that the Hamiltonian does not couple the physical singlet and the unphysical triplet states in the enlarged Hilbert space that is spanned by the spin and the dopon degrees of freedom.[20] A projection to the physical Hilbert space is thus not necessary. We also note here that the dopons, which can be viewed as bound states of spinons and holons in more conventional slave-particle descriptions, carry no gauge charge.

In terms of the spin and dopon operators, the Gutzwiller projected electron operators take the form

$$\tilde{c}^\dagger_{j\sigma} = \frac{\sigma}{\sqrt{2}}\mathcal{P}\big[(1/2 + \sigma S^z_j)d_{j-\sigma} - S^\sigma_j d_{j\sigma}\big]\mathcal{P}\,, \tag{2.3}$$

where S^σ denotes the spin-raising (-lowering) operator S^+ (S^-) for $\sigma = \uparrow(\downarrow)$. From Eq. (2.3), one can easily show that total density of electrons is given by

$$\sum_\sigma \tilde{c}^\dagger_{j\sigma}\tilde{c}_{j\sigma} = \mathcal{P}\left(1 - \sum_\sigma d^\dagger_{j\sigma}d_{j\sigma}\right)\mathcal{P} \overset{\text{lowdoping}}{\approx} 1 - \sum_\sigma d^\dagger_{j\sigma}d_{j\sigma}, \tag{2.4}$$

i.e., the density of doped charge carriers equals the density of dopons $x = \sum_\sigma\langle d^\dagger_{i\sigma}d_{i\sigma}\rangle$, as expected.

As will be explained in more detail in the following, our main assumption is that the localized lattice spins form a $\mathbb{Z}_2$ spin liquid with bosonic spinon excitations. This is reasonably justified in the doping regime close to the antiferromagnetically ordered phase, where the interaction between the lattice spins is frustrated by the motion of dopons. The bosonic nature of the spinons prohibits a hybridization of spinons with fermionic dopons and gives rise to an electronic Fermi surface, the volume of which is determined by the density dopons x alone, as long as no pairing instabilities occur. This is in contrast to the conventional Luttinger theorem, which states that in a metal without broken symmetries, the "volume" enclosed by the Fermi surface should be proportional to the total density of electrons $1 - x$. It has been shown earlier, however, that topological excitations associated with the emergent gauge field of a spin liquid have to be included in the Luttinger count,[14] giving rise to a FL* phase with small-pocket Fermi surfaces, the total volume of which is the same as in an antiferromagnetic metal. In the present formalism, this modified Luttinger theorem of a Fermi surface of size x can be easily proved by applying the usual many-body formalism to the system of interacting spinons and dopons described by Eq. (2.2) [and more explicitly in Eq. (3.3) below]; we need only assume that the final state is adiabatically connected to a state of weakly interacting spinons and dopons, and then the standard proof leads here to the novel Luttinger count of x.

In the presence of strong local antiferromagnetic (AF) correlations, the two important interaction terms between the dopons and the localized spins in Eq. (2.2) are the $\sim\mathbf{S}_i\cdot\mathbf{S}_j$ term, which leads to a strong suppression of nearest-neighbor

hopping of dopons in a locally AF-ordered background, and the $\sim(\mathbf{S}_i + \mathbf{S}_j)$ term, which is responsible for the scattering of dopons with momentum transfer close to $\mathbf{q} = (\pi,\pi)$. In the following, we are going to neglect the $\sim\mathbf{S}_i \times \mathbf{S}_j$ term due to the expected strong local collinear AF correlations. Also, we use a mean-field decoupling of the Heisenberg exchange term in the first line of Eq. (2.2), i.e., $J \to (1-x)^2 J$, and drop the Gutzwiller projectors, which is safe in the low doping limit $x \ll 1$.

III. FL* AND ELECTRON FERMI SURFACE

As mentioned above, the main prerequisite in order to get a fractionalized Fermi liquid is that the localized spins form a spin liquid. Within our model (2.2), spin-liquid ground states can be conveniently described using a Schwinger boson representation for the lattice spins, i.e., we write

$$\mathbf{S}_i = \tfrac{1}{2} b^\dagger_{i\alpha} \boldsymbol{\sigma}_{\alpha\beta} b_{i\beta}, \tag{3.1}$$

which requires the constraint $\sum_\sigma b^\dagger_{i\sigma} b_{i\sigma} = 1$ to hold on every lattice site. Note that there is an emergent U(1) gauge structure associated with the redundancy of the Schwinger boson representation under local phase transformations $b_{j\sigma} \to b_{j\sigma} \exp(i\phi_j)$. The exchange terms can be expressed in terms of Schwinger bosons using the identity

$$\mathbf{S}_i \cdot \mathbf{S}_j = -\frac{1}{2}(\epsilon_{\alpha\beta} b^\dagger_{i\alpha} b^\dagger_{j\beta})(\epsilon_{\gamma\delta} b_{i\gamma} b_{j\delta}) + \frac{1}{4} + \frac{\delta_{ij}}{2}. \tag{3.2}$$

By inserting these expressions in the Hamiltonian (2.2) and using the approximations mentioned above, we obtain the Hamiltonian

$$\begin{aligned} H = &-\frac{1}{4}\sum_{ij}\left[J_{ij} + \frac{t_{ij}}{2}(d^\dagger_{i\alpha} d_{j\alpha} + \text{H.c.})\right] \epsilon_{\alpha\beta} b^\dagger_{i\alpha} b^\dagger_{j\beta}\, \epsilon_{\gamma\delta} b_{i\gamma} b_{j\delta} \\ &+ \frac{1}{2}\sum_{ij}\frac{t_{ij}}{4}[2\, d^\dagger_{i\alpha} d_{j\alpha} - d^\dagger_{i\alpha} d_{j\beta}(b^\dagger_{i\beta} b_{i\alpha} + b^\dagger_{j\beta} b_{j\alpha}) + \text{H.c.}] + \sum_i (\lambda\, b^\dagger_{i\alpha} b_{i\alpha} - \mu\, d^\dagger_{i\alpha} d_{i\alpha}), \end{aligned} \tag{3.3}$$

where λ is the Lagrange multiplier that enforces the Schwinger boson constraint on average. In this representation, a spin liquid can be conveniently described by employing the mean-field decoupling

$$Q_{ij} = \tfrac{1}{2}\langle \epsilon_{\alpha\beta} b^\dagger_{i\alpha} b^\dagger_{j\beta}\rangle. \tag{3.4}$$

This mean-field decoupling preserves the SU(2) invariance since Q_{ij} is a singlet expectation value and gives rise to antiferromagnetic correlations between the spins on sites i and j. We note here that a mean-field decoupling in terms of nonanomalous expectation values would give rise to ferromagnetic correlations between the spins, which is not our case of interest. After a Fourier transformation, we obtain the Euclidean mean-field action [we use the shorthand notation $k = (\omega,\mathbf{k})$]

$$\begin{aligned} S_{\text{MF}}/\beta = &\sum_{k,\sigma} \bar{d}_{k\sigma}(-i\omega_n + \xi^0_{\mathbf{k}}) d_{k\sigma} + \sum_{\mathbf{kq}} Q^*_{\mathbf{k}+\mathbf{q}} J_{\mathbf{q}} Q_{\mathbf{k}} + \sum_k B^\dagger_k \begin{bmatrix} -i\Omega_n + \lambda & -\sum_{\mathbf{p}} Q_{\mathbf{p}} J_{\mathbf{p}-\mathbf{k}} \\ -\sum_{\mathbf{p}} Q^*_{\mathbf{p}} J_{\mathbf{p}-\mathbf{k}} & i\Omega_n + \lambda \end{bmatrix} B_k \\ &- \sum_{q,k,k'} \bar{d}_{k'+q-k\sigma}\, B^\dagger_k\, \mathbf{V}^{\sigma\sigma'}_{\mathbf{k}'\mathbf{kq}}\, B_q\, d_{k'\sigma'} - \frac{1}{2}\sum_{q,k,k'} (t_{\mathbf{k}'} + t_{\mathbf{k}'+\mathbf{q}+\mathbf{k}})[B_{k\downarrow} B_{q\uparrow} \bar{d}_{k+k'+q\uparrow} d_{k'\downarrow} + B^*_{k\uparrow} B^*_{q\downarrow} \bar{d}_{k'\downarrow} d_{k'+k+q\uparrow}], \end{aligned} \tag{3.5}$$

where β denotes the inverse temperature and we have introduced the bosonic Nambu spinor

$$B_k = \begin{pmatrix} b_{k\uparrow} \\ b^*_{-k\downarrow} \end{pmatrix}, \tag{3.6}$$

the interaction matrix

$$\mathbf{V}^{\sigma\sigma'}_{\mathbf{k}'\mathbf{kq}} = \begin{bmatrix} \frac{1}{2}(t_{\mathbf{k}'} + t_{\mathbf{k}'+\mathbf{q}-\mathbf{k}})\delta_{\sigma,\uparrow} & \sum_p Q_{\mathbf{p}}(t_{\mathbf{p}+\mathbf{k}'-\mathbf{k}} + t_{\mathbf{p}-\mathbf{k}'-\mathbf{q}}) \\ \sum_p Q^*_{\mathbf{p}}(t_{\mathbf{p}+\mathbf{k}'-\mathbf{k}} + t_{\mathbf{p}-\mathbf{k}'-\mathbf{q}}) & \frac{1}{2}(t_{\mathbf{k}'} + t_{\mathbf{k}'+\mathbf{q}-\mathbf{k}})\delta_{\sigma,\downarrow} \end{bmatrix} \delta_{\sigma\sigma'}, \tag{3.7}$$

as well as

$$\xi^0_{\mathbf{k}} = t_{\mathbf{k}} + 2\sum_{\mathbf{qp}} Q^*_{\mathbf{q}} t_{\mathbf{p}} Q_{\mathbf{k}+\mathbf{q}-\mathbf{p}} - \mu, \tag{3.8}$$

where $t_{\mathbf{k}}$ is the usual $tt't''$ tight-binding dispersion on the square lattice with nonzero hopping amplitudes up to third nearest neighbors

$$\begin{aligned} t_{\mathbf{k}} = &\, t(\cos k_x + \cos k_y) + t' 2\cos k_x \cos k_y \\ &+ t''(\cos 2k_x + \cos 2k_y). \end{aligned} \tag{3.9}$$

Note that in contrast to $J_{\mathbf{k}}$ and $Q_{\mathbf{k}}$, we have absorbed a factor $1/2$ in the definition of $t_{\mathbf{k}}$. Moreover, $i\omega_n$ and $i\Omega_n$ denote fermionic and bosonic Matsubara frequencies, respectively. Because the bosonic spinon modes are gapped in the spin-liquid phase, we can safely integrate them out and obtain an effective action for the dopon fields d. Expanding to second order in the bosonic propagator, we get

$$\begin{aligned} S^{(2)}_{\text{MF}}[\bar{d},d] = &\, S_0[\bar{d},d] + \text{Tr}\ln\beta\mathcal{G}_0^{-1} - \text{Tr}\,\mathcal{G}_0\Phi - \tfrac{1}{2}\text{Tr}\,\mathcal{G}_0\Phi\mathcal{G}_0\Phi \\ &- \text{Tr}\,\mathcal{G}_0 D\mathcal{G}_0\bar{D} - \text{Tr}\,\mathcal{G}_0\bar{D}\mathcal{G}_0 D, \end{aligned} \tag{3.10}$$

where Tr denotes the trace with respect to momentum, Matsubara, and Nambu indices. Furthermore, we have defined the spinon Green's function

$$\left(\mathcal{G}_0^{-1}\right)_{kq} = \begin{bmatrix} -i\Omega_n + \lambda & -\sum_{\mathbf{p}} Q_{\mathbf{p}} J_{\mathbf{p}-\mathbf{k}} \\ -\sum_{\mathbf{p}} Q_{\mathbf{p}}^* J_{\mathbf{p}-\mathbf{k}} & i\Omega_n + \lambda \end{bmatrix} \delta_{kq} \tag{3.11}$$

and

$$\Phi_{kq} = \sum_{k'} \bar{d}_{k'+q-k\,\sigma} V^{\sigma\sigma'}_{\mathbf{k}'\mathbf{k}\mathbf{q}} d_{k'\sigma'}, \tag{3.12}$$

$$D_{kq} = \frac{1}{4} \sum_{k'} (t_{\mathbf{k}'} + t_{\mathbf{k}'+\mathbf{q}+\mathbf{k}}) \bar{d}_{k'\downarrow} d_{k'+k+q\uparrow}\, \sigma_x, \tag{3.13}$$

$$\bar{D}_{kq} = \frac{1}{4} \sum_{k'} (t_{\mathbf{k}'} + t_{\mathbf{k}'+\mathbf{q}+\mathbf{k}}) \bar{d}_{k'+k+q\uparrow} d_{k'\downarrow}\, \sigma_x, \tag{3.14}$$

where σ_x denotes the respective Pauli matrix in Nambu space. The effective dopon action in Eq. (3.10) describes the hopping of doped charge carriers in a locally AF-ordered background as well as the residual interactions between dopons due to the exchange of a spinon pair. Note, however, that the Schwinger boson mean-field theory presented here can not be used to describe a conventional Fermi liquid state with a large Fermi surface at large doping, where the Luttinger volume is determined by the total density of electrons $1 - x$. This phase can be described using Schwinger fermions instead of bosons.[20] In this case, a hybridization between dopons and fermionic spinons can lead to a ground state with a large Fermi surface.

A. Gaussian dopon action

The linear contribution $\sim\mathcal{G}_0$ to the effective dopon action (3.10) basically descends from the term in the Hamiltonian (2.2) which couples the dopons to $\mathbf{S}_i \cdot \mathbf{S}_j$ and thus strongly renormalizes the bare dopon dispersion. By performing the Matsubara summation and the trace over the Nambu indices of the $\mathrm{Tr}\,\mathcal{G}_0\Phi$ term, we get the Gaussian action

$$\begin{aligned} S^{(1)}_{\mathrm{MF}} = \beta \sum_{k,\sigma} \bar{d}_{k\sigma} \Bigg[& -i\omega_n + \xi^0_{\mathbf{k}} \\ & - \sum_{\mathbf{k}'} \frac{\lambda t_{\mathbf{k}} + 4\sum_{\mathbf{qp}} Q^*_{\mathbf{p}} Q_{\mathbf{q}} J_{\mathbf{q}-\mathbf{k}'} t_{\mathbf{p}+\mathbf{k}-\mathbf{k}'}}{2E_{\mathbf{k}'}} \Bigg] d_{k\sigma} \\ & + \mathrm{Tr}\ln \beta\mathcal{G}_0^{-1} + \beta \sum_{\mathbf{kq}} J_{\mathbf{q}-\mathbf{k}} Q^*_{\mathbf{q}} Q_{\mathbf{k}}. \end{aligned} \tag{3.15}$$

This expression can be simplified using the self-consistency conditions for the Lagrange multiplier λ as well as for the mean field $Q_{\mathbf{k}}$. We make one further approximation here, however, and determine λ and $Q_{\mathbf{k}}$ at the Gaussian level not fully self-consistent, but only with respect to $S^{(0)}_{\mathrm{MF}} = \mathrm{Tr}\ln\beta\mathcal{G}_0^{-1}$, i.e., we neglect the back-action of the dopons on the spinons. The approximate self-consistency equations thus read as

$$0 = \frac{\partial F^{(0)}}{\partial Q^*_{\mathbf{p}}} = \sum_{\mathbf{k}} J_{\mathbf{p}-\mathbf{k}} \left[Q_{\mathbf{k}} - \frac{\sum_{\mathbf{q}} J_{\mathbf{q}-\mathbf{k}} Q_{\mathbf{q}}}{2E_{\mathbf{k}}} \right], \tag{3.16}$$

$$1 = \frac{\partial F^{(0)}}{\partial \lambda} = \sum_{\mathbf{k}} \frac{\lambda}{E_{\mathbf{k}}}, \tag{3.17}$$

where $F^{(0)}$ is the free energy associated with $S^{(0)}_{\mathrm{MF}}$. Here and in the following, $E_{\mathbf{k}}$ denotes the spinon dispersion relation, which is given by

$$E_{\mathbf{k}} = \sqrt{\lambda^2 - \left| \sum_{\mathbf{q}} Q_{\mathbf{q}} J_{\mathbf{q}-\mathbf{k}} \right|^2}. \tag{3.18}$$

By inserting these expressions back into Eq. (3.15), we get

$$S^{(1)}_{\mathrm{MF}} = \beta \sum_{k,\sigma} \bar{d}_{k\sigma} [-i\omega_n + \xi_{\mathbf{k}}]\, d_{k\sigma} + \mathrm{Tr}\ln\beta\mathcal{G}_0^{-1} + \mathrm{const} \tag{3.19}$$

with the Gaussian dopon dispersion

$$\xi_{\mathbf{k}} = t_{\mathbf{k}}/2 - 2\sum_{\mathbf{qp}} Q_{\mathbf{q}} Q^*_{\mathbf{p}} t_{\mathbf{p}+\mathbf{k}-\mathbf{q}} - \mu. \tag{3.20}$$

Note the different sign of the second term compared to the bare dopon dispersion $\xi^0_{\mathbf{k}}$ in Eq. (3.8).

B. Mean-field ansatz for a $\mathbb{Z}_2$ FL*

In the following, we use the simplest mean-field ansatz for the Q_{ij}'s. We take a zero-flux state with $Q_{ij} = Q$ on nearest-neighbor bonds. The invariant gauge group[21] (IGG), i.e., the group of gauge transformations that leaves this ansatz invariant, is U(1) due to the bipartite nature of the square lattice. Indeed, we can choose the gauge transformation $b_{j\sigma} \to b_{j\sigma}\exp(i\phi)$ on sublattice A and $b_{j\sigma} \to b_{j\sigma}\exp(-i\phi)$ on sublattice B without changing the ansatz. However, since a U(1) FL* is generically unstable,[22] we break the U(1) gauge group down to $\mathbb{Z}_2$ by including frustration in the form of a small next-nearest-neighbor exchange interaction J' as well as a corresponding singlet bond amplitude Q'. The excitations of the emergent $\mathbb{Z}_2$ gauge field are gapped visons, which should not play a big role in our subsequent analysis as long as their gap is sufficiently large, thus we neglect them in the following. The Fourier transformation of our ansatz Q_{ij} then takes the form

$$Q_{\mathbf{k}} = i2[Q(\sin k_x + \sin k_y) + 2Q' \cos k_x\, \sin k_y]. \tag{3.21}$$

Note that $Q_{ji} = -Q_{ij}$ and thus $Q_{-\mathbf{k}} = -Q_{\mathbf{k}}$. The corresponding spinon dispersion relation (3.18) is given by

$$E_{\mathbf{k}} = \sqrt{\lambda^2 - 4\,|J\,Q(\sin k_x + \sin k_y) + 2J'Q' \cos k_x \sin k_y|^2}, \tag{3.22}$$

where J and J' are the nearest- and next-nearest-neighbor exchange couplings, whereas Q and Q' are the corresponding singlet amplitudes on nearest- and next-nearest-neighbor bonds. For this choice of $Q_{\mathbf{k}}$, the convolutions in all the expressions for the effective action can be evaluated straightforwardly. In particular, the Gaussian dopon dispersion from Eq. (3.20) takes the form

$$\begin{aligned} \xi_{\mathbf{k}} = {} & \frac{t}{2}(1 - 4|Q|^2)(\cos k_x + \cos k_y) \\ & + t'(1 - 4|Q'|^2)\, \cos k_x \cos k_y \\ & + \frac{t''}{2}(\cos 2k_x + \cos 2k_y) - \mu. \end{aligned} \tag{3.23}$$

Note that the dispersion is invariant under $\mathbb{Z}_2$ gauge transformations $Q_{ij} \to -Q_{ij}$. The singlet amplitudes Q and Q' can

take values between $Q, Q' \in [0,\ 1/\sqrt{2}]$, where $Q = 1/\sqrt{2}$ if nearest-neighbor spins form a singlet. One can clearly see that the nearest-neighbor hopping amplitude vanishes for perfect classical local AF correlations ($Q = 1/2$) and it changes sign for $Q > 1/2$. It is important to emphasize, however, that the Gaussian dopon dispersion (3.23) is strongly renormalized by the residual interaction.

C. Residual interactions, effective dopon action at quartic order

Here, we analyze the interactions between dopons that are induced by the exchange of a spinon pair. The quadratic terms $\sim\mathcal{G}_0^2$ in the effective dopon action (3.10) are given by

$$S_{\rm int}^{(2)} = -\sum_{kq} \mathrm{Tr}_2\Big[\frac{1}{2}(\mathcal{G}_0)_k \Phi_{kq} (\mathcal{G}_0)_q \Phi_{qk} + (\mathcal{G}_0)_k D_{kq} (\mathcal{G}_0)_q \bar{D}_{qk} + (\mathcal{G}_0)_k \bar{D}_{kq} (\mathcal{G}_0)_q D_{qk}\Big]. \tag{3.24}$$

The first term gives rise to non-spin-flip interactions, which we denote by $V^{(1)}_{\mathbf{qkk'}}$, whereas the second and third terms describe interactions where the dopon spins are flipped (denoted by $V^{(2)}_{\mathbf{qkk'}}$). Both interactions are shown schematically in Fig. 1.

In the following, we perform a self-consistent Hartree-Fock analysis of this induced retarded interaction. Self-consistency is necessary because the interactions are strong and the shape as well as the position of the Fermi surface is strongly affected by interaction-induced fluctuations.[23] The Hartree-type interactions are accounted for already to a large extent

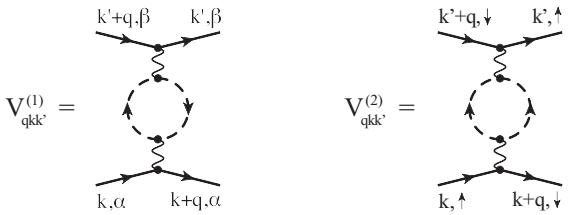

FIG. 1. Dopon-dopon interactions induced by the exchange of a spinon pair.

in the Gaussian dopon dispersion (3.23). In fact, the Hartree diagrams would correspond to a self-energy correction of the bosonic spinon propagator and are not expected to change the results qualitatively. For this reason, we restrict ourselves to the two Fock-type diagrams shown in Fig. 2. Since we expect the Fermi liquid character of the dopons to prevail, we use a dominant pole approximation and neglect the incoherent part of the dopon Green's function. In this approximation, the dressed dopon Green's function in the diagrams in Fig. 2 takes the form

$$G_\sigma(\mathbf{k}, i\omega) \approx \frac{Z_{\mathbf{k}}}{-i\omega + \xi_{\mathbf{k}}}, \tag{3.25}$$

where the quasiparicle residue $Z_{\mathbf{k}}$ as well as the dopon dispersion $\xi_{\mathbf{k}}$ are calculated self-consistently. We will justify this approximation *a posteriori* by checking that the quasiparticle weight $Z_{\mathbf{k}}$ is reasonably large. The dopon self-energy corresponding to the diagrams in Fig. 2 thus takes the form

$$\begin{aligned}\Sigma(\mathbf{k}, i\omega_n) &= \frac{1}{\beta}\sum_q Z_{\mathbf{k+q}} \frac{V^{(1)}_{qkk} + V^{(2)}_{qkk}}{-i\omega_n - i\Omega_q + \xi_{\mathbf{k+q}}} \\ &= -\frac{1}{8\beta^2}\sum_{qk'} Z_{\mathbf{k+q}} \frac{i\Omega_{k'}(i\Omega_{k'} + i\Omega_q)\, a_{\mathbf{kk'q}} + b_{\mathbf{kk'q}}}{[-i\omega_n - i\Omega_q + \xi_{\mathbf{k+q}}]\big[E^2_{k'} - (i\Omega_{k'})^2\big]\big[E^2_{k'+q} - (i\Omega_{k'} + i\Omega_q)^2\big]},\end{aligned} \tag{3.26}$$

where $a_{\mathbf{kk'q}}$ and $b_{\mathbf{kk'q}}$ are momentum-dependent factors given by

$$a_{\mathbf{kk'q}} = 3(t_{\mathbf{k}} + t_{\mathbf{k+q}})^2 - 2|(Q * t)_{\mathbf{k'-k}} + (Q * t)_{\mathbf{k'+k+q}}|^2, \tag{3.27}$$

$$\begin{aligned}b_{\mathbf{kk'q}} = (t_{\mathbf{k}} + t_{\mathbf{k+q}})^2\{3\lambda^2 + [(Q * J)_{\mathbf{k'}}(Q * J)_{\mathbf{k'+q}} + \text{c.c.}]\} + 2\lambda^2|(Q * t)_{\mathbf{k'-k}} + (Q * t)_{\mathbf{k'+k+q}}|^2 + \lambda(t_{\mathbf{k}} + t_{\mathbf{k+q}})[(Q^* * J)_{\mathbf{k'}} \\ + (Q^* * J)_{\mathbf{k'+q}}][(Q * t)_{\mathbf{k'-k}} + (Q * t)_{\mathbf{k'+k+q}}] + \text{c.c.} + (Q^* * J)_{\mathbf{k'}}(Q^* * J)_{\mathbf{k'+q}}[(Q * t)_{\mathbf{k'-k}} + (Q * t)_{\mathbf{k'+k+q}}] + \text{c.c.}\end{aligned} \tag{3.28}$$

Here, the asterisk denotes convolutions, i.e., $(Q * t)_{\mathbf{k}} = \sum_{\mathbf{p}} Q_{\mathbf{p}} t_{\mathbf{k-p}}$.

After performing the Matsubara sums and analytic continuation $i\omega_n \to \omega + i\delta$, we get (at $T = 0$)

$$\begin{aligned}\Sigma_R(\mathbf{k}, \omega) = -\frac{1}{16}\sum_{\mathbf{q},\mathbf{k'}} Z_{\mathbf{k+q}} \Bigg\{ &\frac{1}{2E_{\mathbf{k'}}E_{\mathbf{k'+q}}} \frac{E_{\mathbf{k'}}E_{\mathbf{k'+q}}a_{\mathbf{kk'q}} - b_{\mathbf{kk'q}}}{\omega - E_{\mathbf{k'}} - E_{\mathbf{k'+q}} - \xi_{\mathbf{k+q}} + i\delta} \\ &- \Theta(-\xi_{\mathbf{k+q}})\Bigg[\frac{(E_{\mathbf{k'}} - \xi_{\mathbf{k+q}} + \omega)a_{\mathbf{kk'q}} + b_{\mathbf{kk'q}}/E_{\mathbf{k'}}}{E^2_{\mathbf{k'+q}} - (E_{\mathbf{k'}} - \xi_{\mathbf{k+q}} + \omega + i\delta)^2} + \frac{(E_{\mathbf{k'+q}} + \xi_{\mathbf{k+q}} - \omega)a_{\mathbf{kk'q}} + b_{\mathbf{kk'q}}/E_{\mathbf{k'+q}}}{E^2_{\mathbf{k'}} - (E_{\mathbf{k'+q}} + \xi_{\mathbf{k+q}} - \omega - i\delta)^2}\Bigg]\Bigg\}.\end{aligned} \tag{3.29}$$

The imaginary part of the retarded dopon self-energy finally takes the form

$$\begin{aligned}\mathrm{Im}\Sigma_R(\mathbf{k}, \omega) = -\frac{\pi}{16}\sum_{\mathbf{k'q}} Z_{\mathbf{k+q}} \left(\frac{b_{\mathbf{kk'q}}}{2E_{\mathbf{k'}}E_{\mathbf{k'+q}}} - \frac{a_{\mathbf{kk'q}}}{2}\right) \\ \times[\Theta(\xi_{\mathbf{k+q}})\delta(\omega - E_{\mathbf{k'}} - E_{\mathbf{k'+q}} - \xi_{\mathbf{k+q}}) + \Theta(-\xi_{\mathbf{k+q}})\delta(\omega + E_{\mathbf{k'}} + E_{\mathbf{k'+q}} - \xi_{\mathbf{k+q}})].\end{aligned} \tag{3.30}$$

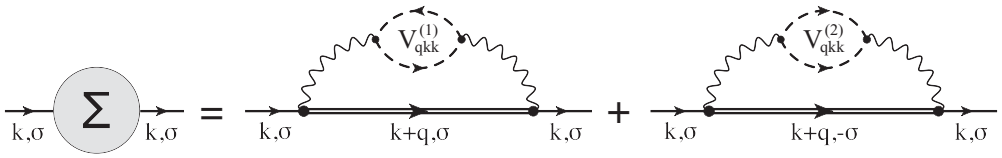

FIG. 2. Fock-type self-energy diagrams for the dopons. Double lines denote dressed dopon Green's functions.

Note that $\mathrm{Im}\Sigma_R(\omega) \equiv 0$ for $-2\Delta < \omega < 2\Delta$, where Δ denotes the spinon gap.

In all subsequent calculations, we do not determine the Lagrange multiplier λ (which fixes the Schwinger boson constraint) self-consistently, but use it to fix the value of the spinon gap Δ. Moreover, we use the nearest- and next-nearest-neighbor singlet amplitudes Q and Q' as free parameters. Our calculation procedure works as follows: first, we evaluate $\mathrm{Im}\Sigma_R(\mathbf{k},\omega)$ numerically using the adaptive Monte Carlo integration algorithm MISER,[24] which is based on a recursive stratified sampling method. Since the computational effort increases considerably with increasing accuracy, we set the bound of the relative error estimate to be smaller than 6%, which is arguably a relatively large value, but sufficient for our purpose. In order to perform the Monte Carlo integration, we smoothen the singularities of the delta functions as well as the step functions by replacing the delta functions by Lorentzians with a full width at half maximum (FWHM) of 0.01 and the step functions by Fermi distributions at an effective inverse temperature $\beta = 200$.

The second step is to evaluate the real part of the self-energy by a Kramers-Kronig transform and determine the dopon dispersion $\xi_{\mathbf{k}}$ by finding the maximum of the dopon spectral function

$$A(\mathbf{k},\omega) = \frac{1}{\pi} \frac{-\mathrm{Im}\Sigma_R(\mathbf{k},\omega)}{\left[-\omega + \xi^{(0)}_{\mathbf{k}} + \mathrm{Re}\Sigma_R(\mathbf{k},\omega)\right]^2 + \left[\mathrm{Im}\Sigma_R(\mathbf{k},\omega)\right]^2}. \tag{3.31}$$

Here, $\xi^{(0)}$ denotes the Gaussian dopon dispersion from Eq. (3.23). The quasiparticle residue $Z_{\mathbf{k}}$ is obtained via

$$Z^{-1}_{\mathbf{k}} = \left| 1 - \frac{\partial\, \mathrm{Re}\Sigma_R(\mathbf{k},\omega)}{\partial\omega} \right|_{\omega=\xi_{\mathbf{k}}}. \tag{3.32}$$

Finally, the self-consistency loop is performed by plugging $\xi_{\mathbf{k}}$ and $Z_{\mathbf{k}}$ back into Eq. (3.30) and repeating the steps above until convergence is achieved.

D. Relation between the electron and the dopon Fermi surface

Using Eq. (2.3), the electron momentum distribution can be expressed in terms of the lattice spin and dopon operators as

$$c^\dagger_{\mathbf{k}\sigma} c_{\mathbf{k}\sigma} = \frac{1}{2} \sum_{ij} e^{i\mathbf{k}\cdot(\mathbf{R}_i - \mathbf{R}_j)} [-(1/4 + \mathbf{S}_i \cdot \mathbf{S}_j) d^\dagger_{j\sigma} d_{i\sigma} + (d^\dagger_{j\alpha} \boldsymbol{\sigma}_{\alpha\beta} d_{i\beta}) \cdot (\mathbf{S}_i + \mathbf{S}_j)/2] + \text{const}, \tag{3.33}$$

where we implicitly sum over repeated spin indices and again neglect the $\mathbf{S}_i \times \mathbf{S}_j$ term. Using the Schwinger boson representation (3.1) for the lattice spins, the electron momentum distribution is given by

$$\begin{aligned} \langle c^\dagger_{\mathbf{k}\sigma} c_{\mathbf{k}\sigma} \rangle &= \frac{1}{2} \sum_{ij} e^{i\mathbf{k}\cdot(\mathbf{R}_i - \mathbf{R}_j)} \Big\langle -d^\dagger_{j\sigma} d_{i\sigma} \\ &\quad + \frac{1}{2} (\epsilon_{\alpha\beta} b^\dagger_{i\alpha} b^\dagger_{j\beta})(\epsilon_{\gamma\delta} b_{i\gamma} b_{j\delta}) d^\dagger_{j\sigma} d_{i\sigma} \\ &\quad + \frac{1}{4} d^\dagger_{j\alpha} d_{i\beta} (b^\dagger_{i\beta} b_{i\alpha} + b^\dagger_{j\beta} b_{j\alpha}) \Big\rangle + \text{const} \\ &= -\frac{1}{2} \langle d^\dagger_{-\mathbf{k}\sigma} d_{-\mathbf{k}\sigma} \rangle + \text{smooth function of } \mathbf{k}. \end{aligned} \tag{3.34}$$

The second line follows because the last two terms give rise to convolutions of the dopon momentum distribution with spinon correlators, where the Fermi surface singularity is smoothened out. We thus conclude that the electron Fermi surface coincides with the dopon Fermi surface. Moreover, the value of the electron quasiparticle residue at the Fermi surface is one-half times the dopon quasiparticle residue $Z_{\mathbf{k}}$.

From Eq. (3.34), it is also clear that the spinon-dopon approach to the t-J model can not give rise to electron pockets at the antinodal regions, as observed in recent experiments. Instead, the Fermi surfaces are always holelike.

E. Results

The following results were obtained using standard values for the bare hopping amplitudes, shown in Table II. The nearest-neighbor hopping amplitude defines our energy scale and has been set to unity. The next-nearest-neighbor exchange interaction J' as well as the corresponding singlet amplitude Q' were chosen to be relatively small compared to the nearest-neighbor values, as their only purpose is to break the IGG form U(1) down to $\mathbb{Z}_2$.

Our results for the self-consistent dopon dispersion $\xi_{\mathbf{k}}$ and quasiparticle residue $Z_{\mathbf{k}}$ as a function of k_x and k_y in the upper right quadrant of the Brillouin zone are shown in Figs. 3–5. These results are at a finite dopon density $n_d > 0$, although we note that $\xi_{\mathbf{k}}$ as well as $Z_{\mathbf{k}}$ look qualitatively similar in the case where the dopon density is going to zero. The position of the dispersion minimum depends on the strength of the local antiferromagnetic correlations, which is parametrized by the singlet bond amplitude Q. For $Q = 1/2$, the hole pockets

TABLE II. Parameter values for hopping amplitudes (t, t', t''), exchange interactions (J, J'), mean-field ansatz bond amplitudes (Q, Q'), as well as for the dopon chemical potential μ and spinon gap Δ.

t	1	J	0.25	Q	Variable	μ	Variable
t'	−0.3	J'	0.05	Q'	0.1	Δ	Variable
t''	0.1						

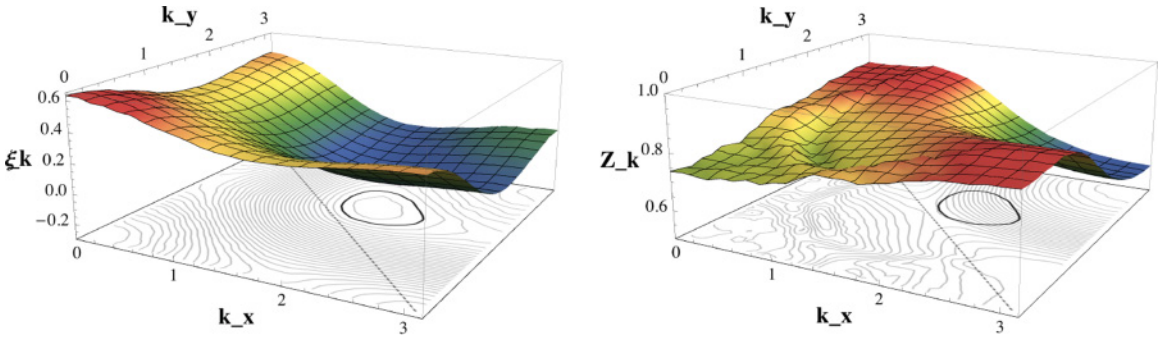

FIG. 3. (Color online) Self-consistent dopon dispersion $\xi_{\mathbf{k}}$ (left) and dopon quasiparticle residue $Z_{\mathbf{k}}$ (right) in the $\mathbb{Z}_2$-FL* phase as a function of k_x and k_y in the upper right quadrant of the Brillouin zone. The thick black contour marks the position of the dopon Fermi surface, which coincides with the electron Fermi surface. The dashed line indicates the magnetic Brillouin zone boundary. Parameter values for this plot are $Q = 0.4$, $\Delta = 0.025$, $\mu = 0.083$, and the rest as in Table II.

are aligned with the magnetic Brillouin zone boundary and centered at $\mathbf{q} \simeq (\pi/2,\pi/2)$. For weaker correlations $Q < 0.5$, the hole pockets are shifted to the outer side of the magnetic Brillouin zone boundary toward $\mathbf{q} = (\pi,\pi)$, whereas stronger local AF correlations $Q > 0.5$ give rise to hole pockets centered on the inner side of the magnetic Brillouin zone boundary (see Fig. 6).

The spinon gap Δ does not influence the position of the pockets, but it changes their shape slightly. The smaller Δ is, the more elliptical are the hole pockets. This is illustrated in Fig. 7. We note, however, that the ellipticity of the hole pockets depends more strongly on the precise value of the bare hopping parameters t' and t'' as on the size of the spinon gap. In fact, smaller t' and t'' give rise to more elliptical pockets, similar to the standard SDW theory for antiferromagnetic metals.

The effective mass of the dopons turns out to be enhanced compared to the bare electron band mass as well. For the two dispersions shown in Fig. 7, the arithmetic mean of the effective masses at the dispersion minimum along the two principal axes is $\bar{m}_{\text{eff}} \approx 2.5$ in natural units (i.e., $m = 1$ corresponds to the band mass of the nearest-neighbor tight-binding dispersion). Again, the effective mass depends on the precise value of the bare hopping parameters t' and t''. For highly elliptical pockets, the effective mass can reach values on the order of $m_{\text{eff}} \sim 10$ along the flat direction.

Within our approximation scheme, the quasiparticle residue $Z_{\mathbf{k}}$ does not drop sharply on the outer half of the Fermi surface, as expected from phenomenological models.[18] Only for relatively high dopon fillings, as in Fig. 3, does an asymmetry of $Z_{\mathbf{k}}$ between the inner and outer sides of the hole pocket appear.

IV. PHASE TRANSITION BETWEEN A $\mathbb{Z}_2$ FL* AND AN AF METAL

The Schwinger boson description (3.1) is well suited to study the quantum phase transition between the $\mathbb{Z}_2$ FL* described above and a metal with long-range antiferromagnetic order. Indeed, SDW ordering corresponds to a condensation of Schwinger bosons at the points where the spinon gap closes, which for $Q' \neq 0$ typically occurs at an incommensurate wave vector. For $Q' = 0$, the spinon dispersion (3.22) has two degenerate minima at the momenta $\mathbf{q} = \pm\mathbf{K}$ with $\mathbf{K} = (\pi/2,\pi/2)$ and the corresponding SDW ordering wave vector is commensurate. A condensate of the two Schwinger boson flavors at these respective momenta, i.e., $\langle b_{\mathbf{q}\uparrow}\rangle = \sqrt{m_s}\,\delta_{\mathbf{q},\mathbf{K}}$ and $\langle b_{\mathbf{q}\downarrow}\rangle = \sqrt{m_s}\,\delta_{\mathbf{q},-\mathbf{K}}$, corresponds to an AF-ordered state with staggered magnetization m_s in the x direction. Note, however, that for $Q' = 0$, the disordered phase no longer corresponds to a $\mathbb{Z}_2$ FL* and thus there is no direct transition between a $\mathbb{Z}_2$ FL* and a commensurate AF-ordered metal.[25] Rather, the transition involves an intermediate incommensurate phase with $Q' \neq 0$; for simplicity, our numerical analysis will not consider this intermediate phase, although the extension is not difficult.

Within our path-integral formulation in Eq. (3.5), a Schwinger boson condensate can be straightforwardly intro-

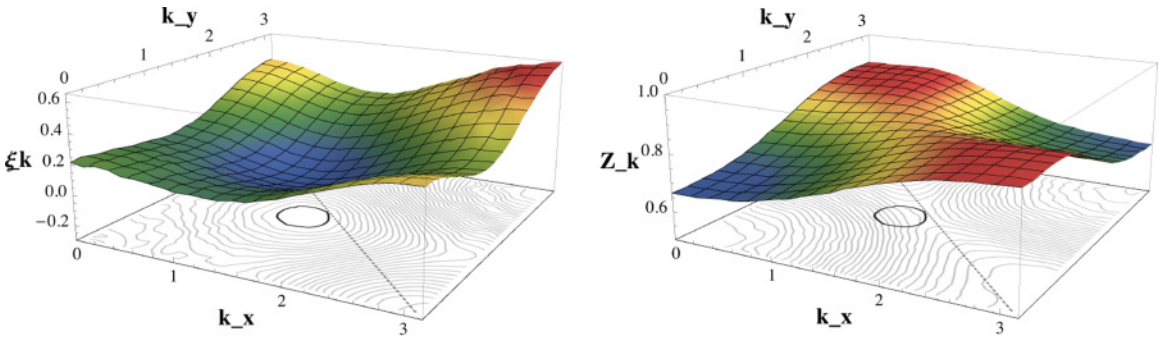

FIG. 4. (Color online) As in Fig. 3, but with parameters $Q = 0.54$, $\Delta = 0.025$, $\mu = 0.18$.

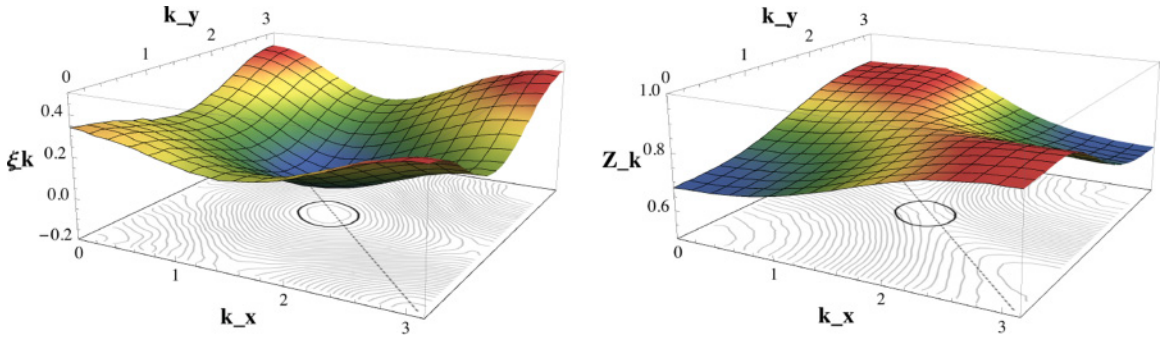

FIG. 5. (Color online) As in Fig. 3, but with parameters $Q = 0.5$, $\Delta = 0.01$, $\mu = 0.182$.

duced by shifting the Nambu fields

$$B_{q\sigma} \to B_{q\sigma} + \sqrt{m_s}\,\delta_{\Omega_n,0}\,\delta_{\mathbf{q},\mathbf{K}} \tag{4.1}$$

and keeping only the quadratic terms in the shifted field. Note that the mean-field ansatz $Q_{\mathbf{k}}$ in Eq. (3.21) also acquires a contribution from the condensate

$$Q_{\mathbf{k}} = \frac{m_s}{2}(\delta_{\mathbf{k},\mathbf{K}} - \delta_{\mathbf{k},-\mathbf{K}}) + Q^{(0)}_{\mathbf{k}}, \tag{4.2}$$

where $Q^{(0)}_{\mathbf{k}} = i2Q(\sin k_x + \sin k_y)$ describes the strong nearest-neighbor correlations on top of the uniform long-range correlations induced by the condensate. The mean-field action in the AF-ordered phase with $\mathbf{K} = (\pi/2,\pi/2)$ has the same form as Eq. (3.5) with three differences. First, $Q_{\mathbf{k}}$ is given by Eq. (4.2). Second, the bare dopon dispersion $\xi^0_{\mathbf{k}}$ in Eq. (3.8) is replaced by

$$\xi^0_{\mathbf{k}} = t_{\mathbf{k}}(1 - m_s) - m_s^2(t_{\mathbf{k}} - t_{\mathbf{k}-\boldsymbol{\pi}}) + 2\sum_{\mathbf{qp}} Q^{(0)*}_{\mathbf{q}} t_{\mathbf{p}} Q^{(0)}_{\mathbf{k}+\mathbf{q}-\mathbf{p}} - \mu, \tag{4.3}$$

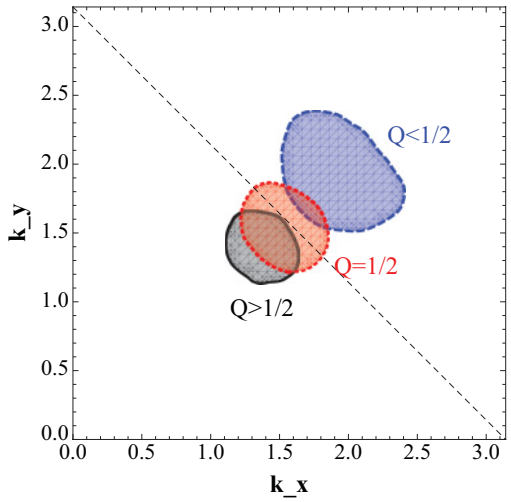

FIG. 6. (Color online) Evolution of the Fermi surface in the $\mathbb{Z}_2$-FL* phase as a function of the nearest-neighbor singlet amplitude $Q \in [0, 1/\sqrt{2}]$. Shown is the upper right quadrant of the Brillouin zone. Black solid line: $Q = 0.54, \Delta = 0.025, \mu = 0.18$; red dotted line: $Q = 0.5, \Delta = 0.01, \mu = 0.182$; blue dashed line: $Q = 0.4, \Delta = 0.025, \mu = 0.083$; other parameters as in Table II. The hole pockets move to the inner side of the magnetic Brillouin zone boundary (indicated by the dashed line) as the strength of local antiferromagnetic correlations, parametrized by Q, increases.

and most importantly, the condensate gives rise to an additional term to the action (3.5), which describes the scattering of dopons with momentum transfer $\mathbf{q} = \boldsymbol{\pi}$ and which takes the form

$$S_{\mathrm{AF}}/\beta = -\frac{m_s}{2}\sum_{\omega_n,\mathbf{k}}(t_{\mathbf{k}} + t_{\mathbf{k}+\boldsymbol{\pi}})(\bar{d}_{\omega_n,\mathbf{k}+\boldsymbol{\pi}\uparrow}\, d_{\omega_n,\mathbf{k}\downarrow} + \mathrm{H.c.}). \tag{4.4}$$

Now, we can perform the same analysis as in Sec. III by integrating out the bosonic modes and performing a Hartree-Fock analysis of the effective quartic dopon action. At this level of approximation, the off-diagonal elements of the self-energy in spin space vanish identically and the diagonal elements have exactly the same structure as in Sec. III. The effective dopon action in the AF-ordered phase including the self-energy corrections is thus given by

$$S/\beta = \sum_k \begin{pmatrix} \bar{d}_{\omega_n,\mathbf{k}+\boldsymbol{\pi}\uparrow} & \bar{d}_{\omega_n,\mathbf{k}\downarrow} \end{pmatrix} \times \begin{bmatrix} \frac{-i\omega_n+\xi_{\mathbf{k}+\boldsymbol{\pi}}}{Z_{\mathbf{k}+\boldsymbol{\pi}}} & -\frac{m_s}{2}(t_{\mathbf{k}} + t_{\mathbf{k}+\boldsymbol{\pi}}) \\ -\frac{m_s}{2}(t_{\mathbf{k}} + t_{\mathbf{k}+\boldsymbol{\pi}}) & \frac{-i\omega_n+\xi_{\mathbf{k}}}{Z_{\mathbf{k}}} \end{bmatrix} \begin{pmatrix} d_{\omega_n,\mathbf{k}+\boldsymbol{\pi}\uparrow} \\ d_{\omega_n,\mathbf{k}\downarrow} \end{pmatrix}, \tag{4.5}$$

where $\xi_{\mathbf{k}}$ and $Z_{\mathbf{k}}$ again denote the self-consistently determined dopon dispersion and quasiparticle residue, calculated in the same manner as in Sec. III using Eqs. (4.2) and (4.3). By diagonalizing (4.5), we obtain two dopon bands with dispersions

$$\omega^{\pm}_{\mathbf{k}} = \frac{\xi_{\mathbf{k}+\boldsymbol{\pi}} + \xi_{\mathbf{k}}}{2} \pm \frac{1}{2}\sqrt{(\xi_{\mathbf{k}+\boldsymbol{\pi}} - \xi_{\mathbf{k}})^2 + m_s^2 Z_{\mathbf{k}} Z_{\mathbf{k}+\boldsymbol{\pi}} (t_{\mathbf{k}} + t_{\mathbf{k}+\boldsymbol{\pi}})^2}. \tag{4.6}$$

The dopon Fermi surface is determined by $\omega^{\pm}_{\mathbf{k}} = 0$. Slightly beyond the AF critical point, where the condensate density is small ($m_s \ll 1$), the self-energy contributions to the dopon Green's function are basically the same as in the $\mathbb{Z}_2$-FL* phase with a vanishing spinon gap and the dispersion $\xi_{\mathbf{k}}$ has a minimum close to $\mathbf{q} = (\pi/2,\pi/2)$, as in Sec. III. The dopon Fermi surface in the AF-ordered phase thus again takes the form of pockets close to $\mathbf{q} = (\pi/2,\pi/2)$. However, the pockets are symmetric with respect to the magnetic Brillouin zone (BZ) boundary due to the presence of long-range antiferromagnetic order. The shape of the hole pocket again depends on the strength of the short-range correlations, parametrized by Q in Eq. (4.2). Possible Fermi surfaces for $m_s = 0.05$ are shown in Fig. 8. For these plots, we used the same $\xi_{\mathbf{k}}$ and $Z_{\mathbf{k}}$ as in the

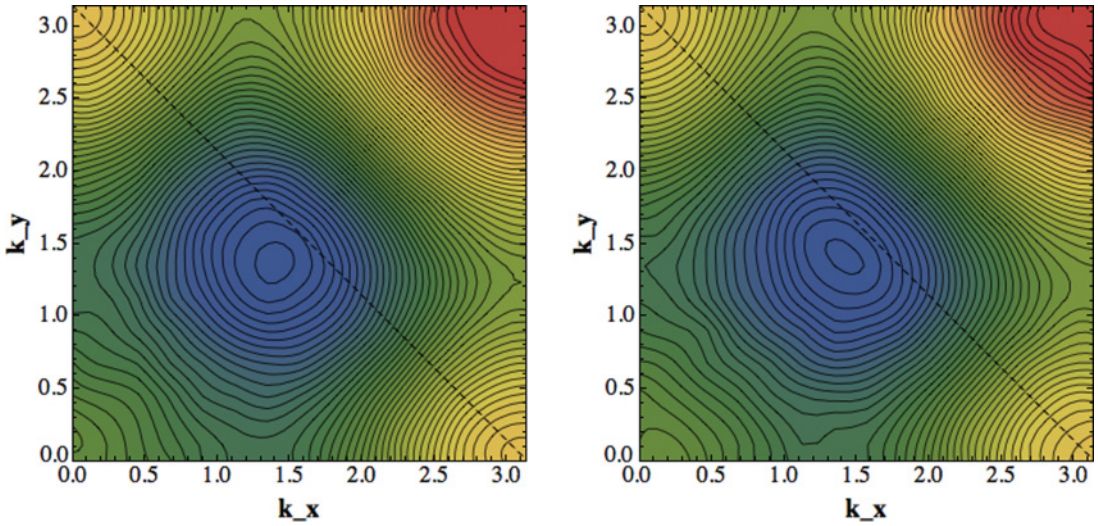

FIG. 7. (Color online) Evolution of the dopon dispersion $\xi_{\mathbf{k}}$ in the $\mathbb{Z}_2$-FL* phase as a function of the spinon gap Δ for $Q = 0.54$ and $\mu = 0.15$. Left: $\Delta = 0.025$; right: $\Delta = 0.005$; other parameters as in Table II. The Fermi energy is below the dopon band in both cases. With decreasing spinon gap Δ, the dispersion around the minima becomes more elliptical.

FL* phase with a vanishingly small spinon gap and $Q' = 0$, which is justified for $m_s \ll 1$, as argued above. Note that for $Q = 1/2$, the dispersion $\xi_{\mathbf{k}}$ is almost symmetric with respect to the magnetic Brillouin zone boundary and thus the two dopon bands in the AF-ordered phase are almost degenerate for $m_s \ll 1$. In this case, we get two concentric Fermi pockets, shown as solid blue and dashed red lines in the left plot of Fig. 8. For larger m_s, the red Fermi pocket shrinks to zero, and we eventually obtain the familiar single hole pocket centered on $\mathbf{q} = (\pi/2,\pi/2)$ of the AF-ordered phase. The right plot shows a Fermi surface for $Q = 0.54$, in which case the single pocket on the inner side of the magnetic BZ in the FL* phase is "symmetrized" at the magnetic BZ boundary.

Note that in the AF-ordered phase, the electron Fermi surface is related to the dopon Fermi surface not by the same Eq. (3.34) as in the FL* phase. The spinon condensate gives rise to additional contributions $\sim m_s$, which only change the electron quasiparticle residue, however. The shape of the electron Fermi surface still coincides with the dopon Fermi surface.

The nature of the quantum-critical point between the AF-ordered and $\mathbb{Z}_2$-FL* phases can be addressed by methods similar to earlier work.[26–29] The magnetic fluctuations are described by the spinor Schwinger bosons, and the critical theory of the transition to a spiral AF-ordered phase is the O(4) Wilson-Fisher fixed point. We now have to check if this critical point is destabilized by the dopon Fermi surfaces. Because the dopons do not carry emergent gauge charges, they couple rather weakly to the critical spin fluctuations;[18] the influence of this coupling can be analyzed perturbatively and, as in previous work,[27,29] it is found to be irrelevant. So the critical theory remains that of the deconfined O(4) variety.[26] In this approach to the onset of magnetic order, there is no direct transition from the $\mathbb{Z}_2$-FL* phase to commensurate AF order, and the latter phase is reached only via an intermediate incommensurate phase.[30]

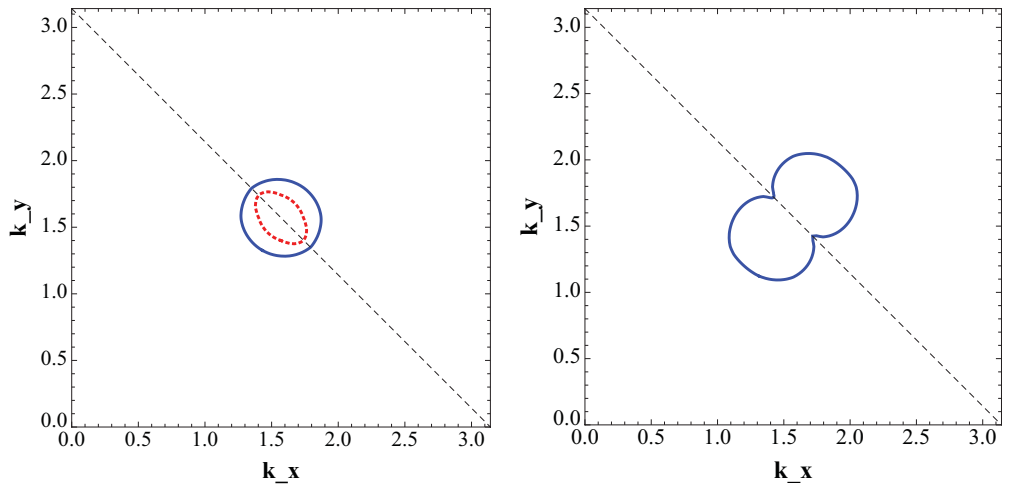

FIG. 8. (Color online) Possible Fermi surface shapes in the antiferromagnetically ordered phase for $m_s \ll 1$. Shown is the upper right quadrant of the Brillouin zone. The dashed line marks the magnetic Brillouin zone boundary. See text for a discussion.

V. CONCLUSIONS

This paper has presented a microscopic construction of a FL* phase in a single-band t-J model on the square lattice, and described its evolution toward the onset of antiferromagnetic order. This was achieved by writing the t-J model in a Kondo-type formulation using the spinon-dopon formalism.[20] The FL* phase had a "background" spin liquid, which was the $\mathbb{Z}_2$ spin liquid with bosonic spinon excitations. This spinon was then coupled to mobile carriers (the "dopons") which had the same quantum numbers of the electron. Our effective Hamiltonian for the spinons and dopons was an exact, in principle, representation of the t-J model. However, we only analyzed this effective Hamiltonian in a relatively straightforward self-consistent one-loop approximation. But, there is an obstacle to extending such an analysis to higher orders and accuracy by using more powerful computational methods.

Our analysis is controlled when the spinon energy gap is large, and it yielded physically sensible results for the electron spectrum that resemble aspects of the experimental observations. The key feature was the presence of a small hole pocket centered near, but *not* at, the magnetic Brillouin zone boundary. This pocket enclosed a volume determined by x, the density of doped carriers alone. The quasiparticle residue was anisotropic around the Fermi surface, but our approximation did not yield the strong variation found in earlier phenomenological models.[18]

We note a recent independent study[31] to describing the underdoped cuprates as a "Luttinger-volume violating Fermi liquid" (LvvFL) with a spin liquid of fermionic spinons. The LvvFL state is qualitatively the same as the FL* state.

On the experimental front, there are a number of recent indications that a FL*-like model of pocket Fermi surfaces without antiferromagnetic long-range order may be appropriate for the pseudogap region of the hole-doped cuprates. The angle dependence of quantum oscillations in $YBa_2Cu_3O_{6.59}$ is consistent[4] with the absence of spin-density-wave ordering. NMR measurements[32] on $YBa_2Cu_3O_y$ have so far not seen antiferromagnetic order at fields as high as 30 T, but do report evidence of charge ordering. Such a charge ordering can be superposed on our FL* analysis in a straightforward manner; as long as the charge ordering wave vector does not connect the hole pockets of the FL* state, there will be little change in the Fermi surface configuration; a computation for the onset of charge order in a FL* metal was described recently by Vojta.[15] We have already noted photoemission evidence for pocket Fermi surfaces.[6]

ACKNOWLEDGMENTS

M.P. gratefully acknowledges numerous discussions with A.-M. S. Tremblay and P. Strack. This research was supported by the National Science Foundation under Grant No. DMR-1103860, and by a MURI grant from AFOSR. M.P. is supported by the Erwin Schrödinger Fellowship J 3077-N16 of the Austrian Science Fund (FWF).

[1] N. Doiron-Leyraud, C. Proust, D. LeBoeuf, J. Levallois, J.-B. Bonnemaison, R. Liang, D. A. Bonn, W. N. Hardy, and L. Taillefer, Nature (London) **447**, 565 (2007).
[2] L. Taillefer, J. Phys.: Condens. Matter **21**, 164212 (2009).
[3] S. E. Sebastian, N. Harrison, P. A. Goddard, M. M. Altarawneh, C. H. Mielke, R. Liang, D. A. Bonn, W. N. Hardy, O. K. Andersen, and G. G. Lonzarich, Phys. Rev. B **81**, 214524 (2010).
[4] B. J. Ramshaw, B. Vignolle, J. Day, R. Liang, W.N. Hardy, C. Proust, and D. A. Bonn, Nature Phys. **7**, 234 (2011).
[5] Hyungju Oh, Hyoung Joon Choi, S. G. Louie, and M. L. Cohen, Phys. Rev. B **84**, 014518 (2011).
[6] H.-B. Yang, J. D. Rameau, Z. H. Pan, G. D. Gu, P. D. Johnson, H. Claus, D. G. Hinks, and T. E. Kidd, Phys. Rev. Lett. **107**, 047003 (2011).
[7] A. J. Millis and M. R. Norman, Phys. Rev. B **76**, 220503(R) (2007).
[8] S. Chakravarty and H.-Y. Kee, Proc. Natl. Acad. Sci. USA **105**, 8835 (2008).
[9] W.-Q. Chen, K.-Y. Yang, T. M. Rice, and F. C. Zhang, Europhys. Lett. **82**, 17004 (2008).
[10] S. Sachdev, A. V. Chubukov, and A. Sokol, Phys. Rev. B **51**, 14874 (1995).
[11] A. V. Chubukov and D. K. Morr, Phys. Rep. **288**, 355 (1997).
[12] M. A. Metlitski and S. Sachdev, Phys. Rev. B **82**, 075128 (2010).
[13] T. Senthil, S. Sachdev, and M. Vojta, Phys. Rev. Lett. **90**, 216403 (2003).
[14] T. Senthil, M. Vojta, and S. Sachdev, Phys. Rev. B **69**, 035111 (2004).
[15] M. Vojta, e-print arXiv:1202.1913.
[16] S. Sachdev, M. A. Metlitski, and M. Punk, e-print arXiv:1202.4760.
[17] S. Burdin, D. R. Grempel, and A. Georges, Phys. Rev. B **66**, 045111 (2002).
[18] Y. Qi and S. Sachdev, Phys. Rev. B **81**, 115129 (2010).
[19] E. G. Moon and S. Sachdev, Phys. Rev. B **83**, 224508 (2011).
[20] T. C. Ribeiro and X.-G. Wen, Phys. Rev. B **74**, 155113 (2006).
[21] X.-G. Wen, Phys. Lett. A **300**, 175 (2002).
[22] N. Read and S. Sachdev, Phys. Rev. Lett. **62**, 1694 (1989).
[23] C. L. Kane, P. A. Lee, and N. Read, Phys. Rev. B **39**, 6880 (1989).
[24] M. Galassi *et al.*, GNU Scientific Library Reference Manual, 3rd ed. (unpublished).
[25] A recent paper (E.-G. Moon and C. Xu, e-print arXiv:1204.5486) has proposed a mechanism for a direct transition from a $\mathbb{Z}_2$ spin liquid to a commensurate antiferromagnet. We expect this has a generalization to a transition from $\mathbb{Z}_2$-FL* state to a commensurate antiferromagnetic metal.
[26] A. V. Chubukov, T. Senthil, and S. Sachdev, Phys. Rev. Lett. **72**, 2089 (1994).
[27] S. Sachdev and T. Morinari, Phys. Rev. B **66**, 235117 (2002).
[28] R. K. Kaul, M. A. Metlitski, S. Sachdev, and C. Xu, Phys. Rev. B **78**, 045110 (2008).
[29] T. Grover and T. Senthil, Phys. Rev. B **81**, 205102 (2010).
[30] C. Xu and S. Sachdev, Phys. Rev. B **79**, 064405 (2009).
[31] Jia-Wei Mei, S. Kawasaki, Guo-Qing Zheng, Zheng-Yu Weng, and X.-G. Wen, Phys. Rev. B **85**, 134519 (2009).
[32] T. Wu *et al.*, Nature (London) **477**, 191 (2011).